J Mol Model (2013) 19:5387–5395
DOI 10.1007/s00894-013-2034-2

ORIGINAL PAPER

Revealing the nature of intermolecular interaction and configurational preference of the nonpolar molecular dimers $(H_2)_2$, $(N_2)_2$, and $(H_2)(N_2)$

Tian Lu · Feiwu Chen

Received: 20 August 2013 / Accepted: 9 October 2013 / Published online: 1 November 2013

Abstract Understanding the nature of noncovalent interactions between nonpolar small molecules is not only theoretically interesting but also important for practical purposes. The interaction mechanism of three prototype dimers $(H_2)_2$, $(N_2)_2$, and $(H_2)(N_2)$ are investigated by state-of-the-art quantum chemistry calculations and energy decomposition analysis. It is shown that their configuration preferences are essentially controlled by the electrostatic component rather than the dispersion effect though the monomers have zero dipole moment. These configuration preferences can also be fairly well and conveniently interpreted by visually examining the electrostatic potential map.

Keywords Coupled cluster · Density functional theory · Electrostatic potential · Energy decomposition · Noncovalent interaction · Quadrupole moment

Introduction

Molecular hydrogen and nitrogen are the most fundamental nonpolar small molecules in the real world. Deeply understanding their intermolecular interaction is not only of theoretical interest but also of huge potential value on practical purposes, such as designing hydrogen storage and nitrogen fixation materials. For a long time, great efforts have been devoted to study the intermolecular interaction of the dimer $(H_2)_2$ [1–11], $(N_2)_2$ [12–21], and $(H_2)(N_2)$ [20–23]. So far, the favorable and unfavorable dimer configurations have been identified, the interaction energies have been computed and even the analytical potential energy surface (PES) has also been built at a high level of quality. However, the nature of the inter-monomer interaction has not been well understood and in particular, rare papers focus on elucidating the reason why the favorable configurations of the homodimers and the heterodimer are so different — the most favorable configurations of $(H_2)_2$ and $(N_2)_2$ are T and Z shapes, whereas the most favorable and unfavorable configurations of $(H_2)(N_2)$ are L and T, respectively (See Fig. 1 for illustration). In this study, we aim to convey a definitive insight into the interaction nature of the three dimers. The highest level of calculation on the interaction energies of these three dimers will be presented, meanwhile energy decomposition technique, quadrupole-quadrupole interaction model and a visualization scheme based on the molecular electrostatic potential will be employed to unveil the major factor controlling the stability sequence of the dimer configurations.

Computational details

Five representative configurations were taken into account for each dimer. The geometry optimization and harmonic vibrational frequency analysis for the three dimers were carried out at MP2 level by Gaussian 03 program [24], H-H and N-N bond lengths were free to relax during the optimization. aug-cc-pVTZ [25, 26] and jun-cc-pVTZ [27] basis sets were applied for hydrogen and nitrogen, respectively. jun-cc-pVTZ is a modified version of aug-cc-pVTZ by removing its *f*-type diffusion basis function. This modification significantly facilitates the convergence of the geometry optimization process while the loss of accuracy is trivial [27].

Electronic supplementary material The online version of this article (doi:10.1007/s00894-013-2034-2) contains supplementary material, which is available to authorized users.

T. Lu · F. Chen (✉)
Department of Chemistry and Chemical Engineering, School of Chemistry and Biological Engineering, University of Science and Technology Beijing, Beijing 100083, People's Republic of China
e-mail: chenfeiwu@ustb.edu.cn

T. Lu · F. Chen
Beijing Key Laboratory for Science and Application of Functional Molecular and Crystalline Materials, Beijing 100083, People's Republic of China

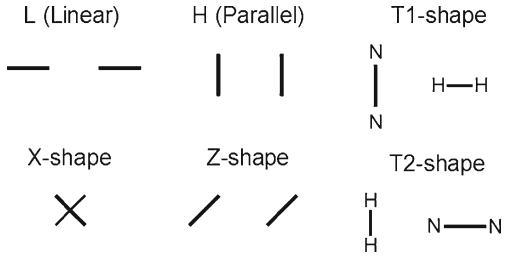

Fig. 1 Illustration of typical configurations of the dimer $(H_2)_2$, $(N_2)_2$, and $(H_2)(N_2)$. The heterodimer $(H_2)(N_2)$ has two different T-shape configurations, which are referred to as T1 and T2, respectively

The MP2 and CCSD(T) intermolecular interaction energies at the optimized structures were calculated by Gaussian 03 program, aug-cc-pVnZ (n=T, Q) were used to extrapolate the result to complete basis-set (CBS) limitation [28]. Basis-set superposition error (BSSE) was corrected by counterpoise method [29]. As a comparison, the interaction energies are also assessed by some popular density functional theory (DFT) methods, including PBE [30], B3LYP [31], M06-2X [32], M11 [33], and two dispersion corrected methods B3LYP-D3 [34] (B3LYP with Grimme's DFT-D3 correction) and ωB97X-D [35]. All of the DFT calculations were realized by GAMESS-US version 1 MAY 2013 [36] in conjunction with aug-cc-pVQZ. Since it is well known that self-consistent field (SCF) energy converges much faster than post-HF energy with respect to basis sets [37], meanwhile the aug-cc-pVQZ is sufficiently large and almost free of the BSSE problem, the basis set extrapolation and counterpoise correction were omitted for the DFT calculations. A very recently proposed semi-empirical method PM7 [38], which was proven to be able to deal with noncovalent interaction problems rather well, was also employed to evaluate the interaction energy by using MOPAC 2012 program [39].

Via Molpro 2008 package [40], the interaction energies were computed and further decomposed into physical components by second-order DFT-SAPT scheme [41, 42]. PBE0 exchange-correlation functional [43] in combination with aug-cc-pVTZ was used in the calculation. More details about the DFT-SAPT method can be found in "Results and discussion" of the supplemental material.

Based on the electron density produced at MP2/aug-cc-pVTZ level, the electrostatic potential maps and deformation maps of electron density of H_2 and N_2 were plotted by Multiwfn 3.1 program [44, 45].

Results and discussion

Interaction energies and stable configurations

The interaction energies, the imaginary frequencies or the lowest real frequency of the representative configurations of $(H_2)_2$, $(N_2)_2$, and $(H_2)(N_2)$ are summarized in Table 1, the entries were ranked according to CCSD(T) interaction energies. Optimized geometry coordinates and complete vibrational frequencies are provided in "Introduction" and "Computational details" of the supplemental material, respectively.

From the $\Delta E_{CCSD(T)}$ shown in the table, it can be seen that for $(H_2)_2$ and $(N_2)_2$, the stability sequences of the configurations are basically the same, namely T≈Z>X>H>L. Vibrational frequency analysis shows that the only real PES minima of $(H_2)_2$ and $(N_2)_2$ are T and Z configurations, respectively. For the latter, the lowest frequency (0.8 cm^{-1}) is quite close to zero, the corresponding vibrational mode points to T configuration, implying that the minimum energy path connecting T and Z shapes of $(N_2)_2$ is considerably flat. Relative to the two homodimers, the configurational stability of $(H_2)(N_2)$ is completely inverted, namely L>H>X>T1>T2, in which L shape is the only PES minimum since no imaginary frequency appears. Note that Z shape of $(H_2)(N_2)$ cannot be obtained because it is not a minimum and proper symmetry constraint was unable to be imposed during the optimization.

In the dimer environment, the geometry of the monomers deform relative to their free states. The variations of the bond lengths of the two monomers are given in Table 1 as ΔR_1 and ΔR_2. The free-state bond length H-H=0.73744 Å and N-N=1.11408 Å were obtained at the same level as the dimer optimizations. It can be seen that the bond length variations are quite small for both H-H and N-N bonds. The maximal variation is much less than 0.001 Å. Therefore freezing the monomer structures in the dimer studies, as many literature works did, can be regarded as a reasonable approximation.

The interaction energies derived at the CCSD(T)/CBS level is a well recognized gold standard to assess the accuracy of other computational methods [46]. In order to examine the performances of different approaches, the interaction energies of the representative configurations of $(H_2)_2$, $(N_2)_2$ and $(H_2)(N_2)$ calculated by various theoretical methods are listed in Table 2. From Table 2 it can be seen that MP2 underestimated interaction energy for $(H_2)_2$, but evidently overestimated interaction energy for $(N_2)_2$. For $(H_2)(N_2)$, probably due to the fortuitous error cancellation, the error is small. The stability sequence predicted by MP2 is totally correct for $(H_2)_2$ and $(H_2)(N_2)$, but not for $(N_2)_2$. Therefore it is safe to use MP2 to qualitatively study $(H_2)_2$ and $(H_2)(N_2)$, however, in order to investigate $(N_2)_2$, this popular method should be used with caution.

So far very few literature works [18, 47, 48] attempt to employ DFT methods to study the noncovalent interaction of $(H_2)_2$, $(N_2)_2$ and $(H_2)(N_2)$. This is because DFT methods are in general unable to achieve highly accurate calculations and a large number of conventional exchange-correlation

Table 1 Center-to-center distance ($R_{c\text{-}c}$), variation of bond length of monomer 1 and 2 relative to their free-states (ΔR_1 and ΔR_2), imaginary frequencies (negative values) or the lowest real frequency, as well as CCSD(T) interaction energies of the representative configurations of $(H_2)_2$, $(N_2)_2$, and $(H_2)(N_2)$[a]

Dimer	Config.	$R_{c\text{-}c}$	ΔR_1	ΔR_2	Freq. (cm^{-1})[b]	$\Delta E_{CCSD(T)}$
$(H_2)_2$	L (D_∞)	3.721	−0.03	−0.03	$(-87.4)_D$	−9.7
	H (D_{2h})	3.678	−0.01	−0.01	−93.0, −45.1, −34.2	−12.2
	X (D_{2d})	3.585	0.01	0.01	$(-64.8)_D$	−16.9
	Z (C_{2h})	3.435	0.11	0.11	−34.0	−33.4
	T (C_{2v})	3.405	0.13	0.13	50.5	−36.2
$(N_2)_2$	L (D_∞)	4.739	0.15	0.15	$(-36.1)_D$, $(-8.4)_D$	−19.2
	H (D_{2h})	3.566	0.23	0.23	−21.2, −14.5	−71.7
	X (D_{2d})	3.529	0.15	0.15	$(-9.2)_D$	−84.3
	T (C_{2v})	4.031	0.04	0.02	−10.0	−97.0
	Z (C_{2h})	3.903	0.08	0.08	0.8	−102.8
$(H_2)(N_2)$	T2 (C_{2v})	4.131	−0.04	0.05	−131.2, −5.9, −5.7	−20.0
	T1 (C_{2v})	3.483	−0.02	0.09	−37.9	−28.0
	X (C_{2v})	3.440	0.09	0.03	−55.9, −41.7	−48.2
	H (C_{2v})	3.414	0.19	0.02	−55.6	−57.5
	L (C_∞)	3.871	0.45	−0.03	$(27.1)_D$	−70.8

[a] Energies are given in cm^{-1} ($1\ cm^{-1} = 0.012\ kJ\ mol^{-1}$), $R_{c\text{-}c}$ are given in Å, while ΔR_1 and ΔR_2 are shown in 10^{-3} Å. For $(H_2)(N_2)$, monomer 1 and 2 denote H_2 and N_2, respectively. The monomers at their dimer geometries were taken as reference to derive the interaction energies

[b] The subscript D means the vibrational frequencies are doubly degenerated

functionals totally fail to reproduce dispersion interaction [46]. However, more and more new DFT methods proposed in recent years were explicitly optimized for noncovalent interaction, thus it would be interesting and meaningful to examine whether they are applicable to the dimers studied here. From Table 2 it is obvious that the most widely used functional B3LYP is completely useless, which even predicts the dimers to be unbound. Compared to B3LYP, PBE performs much better, at least the most stable configurations are correctly identified, and the corresponding interaction energies are all negative. It is known that M06-2X in general gives very good results for noncovalent interaction [46], and indeed it correctly reproduces the stability sequence for H_2 dimer. However, it does not have the ability to reproduce the

Table 2 Interaction energies (cm^{-1}) of the representative configurations of $(H_2)_2$, $(N_2)_2$ and $(H_2)(N_2)$ calculated by various theoretical methods

Dimer	Config.	ΔE_{MP2}	ΔE_{PBE}	ΔE_{B3LYP}	$\Delta E_{M06\text{-}2X}$	ΔE_{M11}	$\Delta E_{\omega B97X\text{-}D}$	$\Delta E_{B3LYP\text{-}D3}$	ΔE_{PM7}
$(H_2)_2$	L (D_∞)	−4.7	−25.8	36.7	−24.7	18.8	−6.9	−1.6	−21.6
	H (D_{2h})	−8.0	−21.5	30.0	−34.7	6.9	−12.4	−0.8	−18.0
	X (D_{2d})	−12.2	−27.1	30.2	−38.1	4.2	−16.1	−5.2	−16.3
	Z (C_{2h})	−27.9	−48.0	25.7	−41.8	8.5	−27.7	−23.9	−18.3
	T (C_{2v})	−30.5	−50.6	25.3	−42.8	6.2	−30.2	−26.1	−19.0
$(N_2)_2$	L (D_∞)	−32.3	2.8	86.6	−6.2	7.8	20.2	2.1	59.6
	H (D_{2h})	−124.4	23.8	157.0	−38.7	−9.4	−12.0	−54.3	17.6
	X (D_{2d})	−132.1	10.0	145.9	−51.1	−30.1	−29.2	−72.7	−55.5
	T (C_{2v})	−129.1	−36.5	80.1	−47.2	−30.1	−23.6	−74.1	−205.1
	Z (C_{2h})	−140.4	−41.3	81.9	−37.2	−11.2	−15.8	−92.2	−197.5
$(H_2)(N_2)$	T2 (C_{2v})	−17.2	−21.6	51.2	−29.0	9.3	−7.2	−6.6	−37.2
	T1 (C_{2v})	−30.2	−15.9	86.2	−19.6	11.0	−9.1	−26.0	−40.3
	X (C_{2v})	−51.6	−32.9	67.0	−45.8	−7.3	−32.1	−39.9	−36.9
	H (C_{2v})	−64.3	−39.2	63.7	−48.8	−10.0	−37.1	−46.8	−35.0
	L (C_∞)	−76.6	−71.0	28.5	−33.7	−15.8	−25.2	−63.6	−40.8

sequence for $(N_2)_2$ and $(H_2)(N_2)$. The result of recently proposed Minnesota functional M11 is very disappointing and much worse than its predecessor M06-2X. Both ωB97X-D and B3LYP-D3 are the DFT functionals with the Grimme's DFT-D dispersion correction term. We found that the former one performs well for $(H_2)_2$ while the latter one gives quite a satisfactory result for $(N_2)_2$ and $(H_2)(N_2)$. In summary, according to the test data it can be seen that accurately evaluating the interaction energies for $(H_2)_2$, $(N_2)_2$, and $(H_2)(N_2)$ is still a difficult problem for existing DFT functionals. Among the ones we tested, B3LYP-D3 has the best overall performance, which successfully reproduces the stability sequence for all of the three dimers, and its quantitative error of interaction energies relative to CCSD(T) are in tolerable range. So it is expected that B3LYP-D3 could be an ideal choice to investigate the clusters comprising a large number of H_2 and N_2. We also examined the new semi-empirical method PM7, which also takes dispersion correction into account to enhance its capability for noncovalent interaction problems; unfortunately, it is seen from these test data that its error is too large to be applied to study the dimers.

Energy decomposition analysis

Because of the zero dipole moment of H_2 and N_2, it is the general belief that $(H_2)_2$, $(N_2)_2$, and $(H_2)(N_2)$ are typical van der Waals (vdW) dimers, namely the dispersion effect dominates the inter-monomer interaction. However, from dispersion effect point of view, the clear difference of the configurational stability between the homodimer and heterodimer can hardly be properly explained. The energy components derived by second-order DFT-SAPT [42] allow one to gain a deeper insight into the nature of the interaction. The results of the DFT-SAPT analysis are given in Table 2. The DFT-SAPT interaction energy ΔE_{SAPT} is the sum of electrostatic (ΔE_{ele}), dispersion (ΔE_{disp}), exchange repulsion (ΔE_{ex}), induction (ΔE_{ind}) and δHF terms, where δHF is a trivial term used to take higher order effects into account [42].

We first note that the interaction energies ΔE_{SAPT} in Table 3 are quite close to those $\Delta E_{CCSD(T)}$ in Table 1 calculated at the expensive CCSD(T)/CBS+ counterpoise level, and their predicted configurational stability sequences are also fully identical, suggesting that DFT-SAPT is an efficient and reliable approach to study small weakly bound dimers. The most striking finding from the DFT-SAPT calculation is that the sequence of electrostatic interaction terms in the table is in complete accord with the sequence of total interaction energies $\Delta E_{CCSD(T)}$ for all three dimers. This is not a coincidence, since the numerical difference of the electrostatic term between each configuration is large enough to distinguish the relative configurational stability. Meanwhile we noted that all of the most unstable configurations have a positive ΔE_{ele} value, indicating that the electrostatic effect plays a pure repulsive role in these cases. Compared to the electrostatic terms, the dispersion terms always have values in a much larger magnitude, as if the attractive inter-monomer interactions are indeed solely dominated by the dispersion effect. However, the correlation between ΔE_{disp} and total interaction energies seems unclear. If the exchange-repulsion terms are combined into dispersion terms as $\Delta E_{exc+disp}$, then their values are significantly cancelled out and are comparable to ΔE_{ele} in magnitude. Nevertheless, the sequence of $\Delta E_{ex+disp}$ is still in a wrong order in comparison with the dimer's total interaction energies. Mainly because the monomer is neutral and nonpolar, the induction term is very small and incapable of affecting the relative stability of the

Table 3 Physical components of the interaction energies (cm^{-1}) of the representative configurations of $(H_2)_2$, $(N_2)_2$, and $(H_2)(N_2)$ derived by DFT-SAPT method

Dimer	Config.	ΔE_{SAPT}	ΔE_{ele}	ΔE_{exc}	ΔE_{disp}	$\Delta E_{exc+disp}$	ΔE_{ind}	δHF
$(H_2)_2$	L (D_∞)	−12.5	12.2	22.0	−43.4	−21.4	−1.4	−1.8
	H (D_{2h})	−13.2	3.4	13.0	−28.9	−15.9	−0.2	−0.5
	X (D_{2d})	−17.9	−1.2	18.0	−33.7	−15.7	−0.2	−0.7
	Z (C_{2h})	−35.4	−17.8	42.8	−56.4	−13.6	−1.2	−2.8
	T (C_{2v})	−38.3	−21.4	47.9	−59.9	−12.1	−1.6	−3.2
$(N_2)_2$	L (D_∞)	−22.3	19.9	77.0	−115.4	−38.5	−1.7	−2.0
	H (D_{2h})	−72.5	−22.3	194.5	−238.5	−44.0	−1.9	−4.3
	X (D_{2d})	−84.0	−39.4	206.1	−243.1	−37.1	−2.2	−5.3
	T (C_{2v})	−93.5	−70.5	184.0	−199.3	−15.3	−2.3	−5.5
	Z (C_{2h})	−100.0	−73.0	212.1	−223.4	−11.3	−3.1	−12.6
$(H_2)(N_2)$	T2 (C_{2v})	−21.3	4.7	41.2	−65.1	−23.9	−0.7	−1.4
	T1 (C_{2v})	−32.0	−5.7	111.8	−129.1	−17.3	−3.3	−5.8
	X (C_{2v})	−48.6	−25.5	91.8	−111.0	−19.2	−0.9	−2.9
	H (C_{2v})	−57.3	−36.5	102.2	−118.7	−16.5	−1.0	−3.3
	L (C_∞)	−69.6	−73.3	151.2	−134.2	17.1	−5.0	−8.4

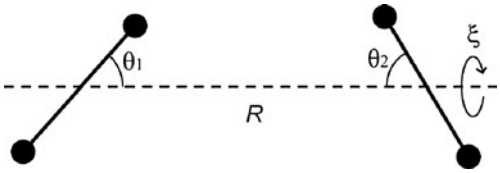

Fig. 2 The definition of the geometry variables in dimer systems

configurations. Based on above observations, it can be concluded that the configurational preference of $(H_2)_2$, $(N_2)_2$, and $(H_2)(N_2)$ is essentially controlled by the electrostatic effect. Besides, for the relatively stable configurations, one can see from the data shown in Table 2 that the electrostatic attraction is indispensable or the most important momentum of dimerization. Therefore taking these dimers as "van der Waals complex", as many literature and textbooks did [17, 20, 22], may be not entirely appropriate, at least the importance of electrostatic effect is seriously underestimated.

Quadrupole moment interaction

Now a question naturally arises: How does the electrostatic interaction lead to so different configurational preferences for the homodimer and heterodimer? What is the physical picture behind these phenomena?

Quadrupole moment is the lowest order of non-vanished electric multipole moment of H_2 and N_2. Therefore, the quadrupole-quadrupole interaction is the most simplified model to study the electrostatic component of the intermolecular interaction, which may shed some light on the above question. This point of view has been used to discuss the configurational preference of homodimers [49].

For H_2 or N_2, assume that the molecular axis parallels the Z axis, then its quadrupole moment can be simply represented as a scalar quantity Θ [50], which equals to the ZZ component of the traceless quadrupole moment tensor. Θ is indicative of the deviation of charge distribution from spherical symmetry. The more positive (negative) the Θ is, the more strongly the electron density distribution contracts (elongates) along the molecular axis. The Θ of H_2 and N_2 computed at MP2/aug-cc-pVTZ level are 0.472 and −1.180 a.u., respectively, which are in good agreement with the corresponding experimental values 0.460±0.021 [51] and −1.15 a.u. [52]. The great difference in magnitude and in sign of Θ of H_2 and N_2 suggests the conspicuous difference of their electron density distribution, which will be discussed later.

If we define the geometry variables in dimer systems as Fig. 2, then the quadrupole-quadrupole interaction energy $E_{\Theta\Theta}$ between the two monomers can be calculated as follows [50],

$$E_{\Theta\Theta} = \frac{3\Theta_1\Theta_2}{4R^5}\Big(1-5\cos^2\theta_1-5\cos^2\theta_2+17\cos^2\theta_1\cos^2\theta_2 + 2\sin^2\theta_1\sin^2\theta_2\cos^2\zeta+16\sin\theta_1\sin\theta_2\cos\theta_1\cos\theta_2\cos\zeta\Big) \quad (1)$$

The results of $E_{\Theta\Theta}$ for $(H_2)_2$, $(N_2)_2$ and $(H_2)(N_2)$ are listed in Table 4. In order to get rid of the influence of the different intermolecular distances R in various configurations, the $E_{\Theta\Theta}$ are also calculated at average intermolecular distance.

From Table 4 it can be seen that the quantitative data of $E_{\Theta\Theta}$ deviate from the ΔE_{ele} terms of DFT-SAPT analysis apparently because all higher-order of electric multipole moments are omitted and the R is not very large. Nevertheless, the sequence of $E_{\Theta\Theta}$ shows obvious correlation with the sequence of configuration stability. If the $E_{\Theta\Theta}$ are calculated at fixed R, the stability sequences for all dimers are basically correct. But the T-shape of $(N_2)_2$ is predicted to be too stable, and the relative stability of T1 and T2 of $(H_2)(N_2)$ are unable to be discriminated, reflecting the limitation of quadrupole-quadrupole interaction model. Notice that $E_{\Theta\Theta}$ is sensitive to the choice of R, if the optimized R are used, the inter-monomer repulsion in H-shape of $(N_2)_2$ and T1-shape of $(H_2)(N_2)$ will be greatly exaggerated.

The expression of Eq. 1 in conjunction with Table 4 is enough to qualitatively explain the reason why the homodimers prefer T or Z-shape, while the heterodimer prefers L configuration. Since the prefactor in Eq. 1 is always positive for homodimers and the sum of the terms in the parenthesis of

Table 4 Quadrupole-quadrupole interaction energies for different configurations of $(H_2)_2$, $(N_2)_2$ and $(H_2)(N_2)$, the configurations are ranked according to CCSD(T) interaction energy[a]

$(H_2)_2$			$(N_2)_2$			$(H_2)(N_2)$		
Config.	$E_{\Theta\Theta}(R_{opt})$	$E_{\Theta\Theta}(R_{avg})$	Config.	$E_{\Theta\Theta}(R_{opt})$	$E_{\Theta\Theta}(R_{avg})$	Config.	$E_{\Theta\Theta}(R_{opt})$	$E_{\Theta\Theta}(R_{avg})$
L (D_∞)	17.1	21.2	L (D_∞)	31.8	78.7	T2 (C_{2v})	12.7	22.9
H (D_{2h})	6.8	7.9	H (D_{2h})	49.4	29.5	T1 (C_{2v})	29.7	22.9
X (D_{2d})	2.6	2.6	X (D_{2d})	17.4	9.8	X (C_{2v})	−7.9	−5.7
Z (C_{2h})	−10.4	−8.6	T (C_{2v})	−35.7	−39.3	H (C_{2v})	−24.6	−17.2
T (C_{2v})	−13.3	−10.6	Z (C_{2h})	−35.9	−33.6	L (C_∞)	−35.0	−45.8

[a] The values are given in cm^{-1}. $E_{\Theta\Theta}(R_{opt})$ and $E_{\Theta\Theta}(R_{avg})$ denote the interaction energies calculated at MP2 optimized intermolecular distance (R_{opt}) and at the average distance of the five configurations (R_{avg}), respectively. R_{avg} of $(H_2)_2$, $(N_2)_2$, and $(H_2)(N_2)$ are 3.564, 3.954, and 3.668 Å, respectively

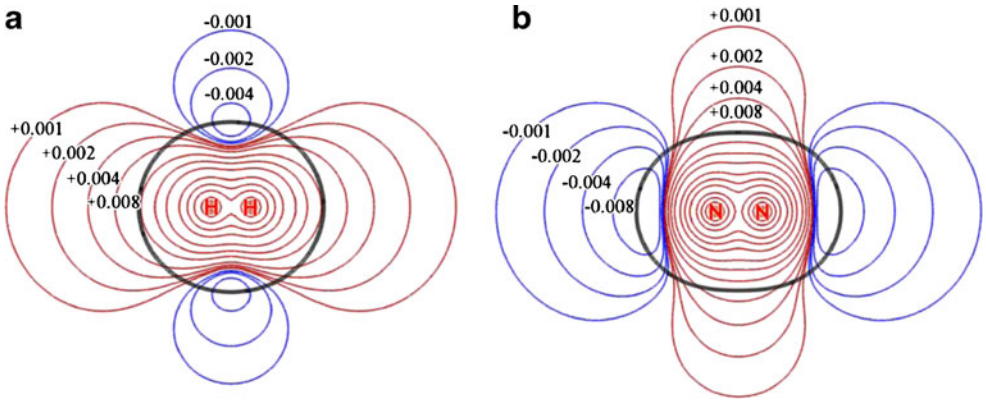

Fig. 3 ESP map of H_2 (**a**) and N_2 (**b**). Positive and negative parts are represented as red and blue lines, respectively. The black lines correspond to Bader's vdW surface, namely the isosurface of ρ=0.001 a.u. The unit of the labeled contours is in a.u.

Eq. 1 is negative only for T and Z configurations, their product will give rise to a negative value of $E_{\Theta\Theta}$, which mean that T and Z configurations are more stable. Due to the different sign of Θ of H_2 and N_2, the prefactor in Eq. 1 is negative for the heterodimer. Because the sum of the terms in the parenthesis of Eq. 1 has the largest positive value for L configuration, the L-shape of $(H_2)(N_2)$ with the largest negative value of $E_{\Theta\Theta}$ is expected to be most stable.

Electrostatic potential analysis

The quadrupole moment analysis in the last section indeed provides a useful insight into the intermolecular interaction of $(H_2)_2$, $(N_2)_2$, and $(H_2)(N_2)$. However, this analysis is more or less abstract and does not provide an intuitive picture to understand these interactions. Also, one should bear in mind that the quadrupole moment is only the crudest approximation of charge distribution of nonpolar molecules. In this section, we will investigate the configuration preference based on the electrostatic potential (ESP) analysis [53–57], which is not only more intuitive but also more rigorous. It is noteworthy that ESP distribution of many nonpolar small molecules were quantitatively characterized by Brinck et al. about 20 years ago [58]. Although they did not discuss ESP of H_2 and N_2 in detail, their data implied that the ESP distribution on the vdW surface of H_2 and N_2 is highly anisotropic.

First let us take a look at the electrostatic potential map of the monomers, H_2 and N_2, as shown in Fig. 3. The black lines correspond to Bader's vdW surface [59]. Since only the region outside vdW surface is of interest, the region enclosed by the black bold line will thus not be concerned. From these maps, one can immediately capture the striking difference between these two molecules. For H_2, the positive ESP region is distributed along the molecular axis, while negative region encircles the axis. The status of N_2 is entirely opposite to that of H_2, namely evident negative ESP regions occur at both sides of the molecular axis, and meanwhile the axis is encompassed by positive ESP zone. The different ESP distribution of H_2 and N_2 closely relates to their different sign of quadrupole moment.

The formation of the strong anisotropic character of ESP of H_2 and N_2 can be understood by means of deformation map of electron density, see Fig. 4. The negative ESP region encircling H_2 axis arises from the negative contribution of the electrons concentrated in the H-H bonding region. The ESP at both ends of the molecular axis of H_2 becomes positive due to the descreening of the nuclear charges. For N_2, Fig. 4b shows that during formation of the molecule, a large amount of electron density concentrates in the lone pair region. This is why N_2 has very negative ESP at both sides of its molecular axis. Due to the triple bond, the electron density between the two nitrogen nuclei is increased, while the electron density in the planes perpendicular to the molecular axis and crossing the nuclei is decreased. As illustrated in Fig. 5, this change of

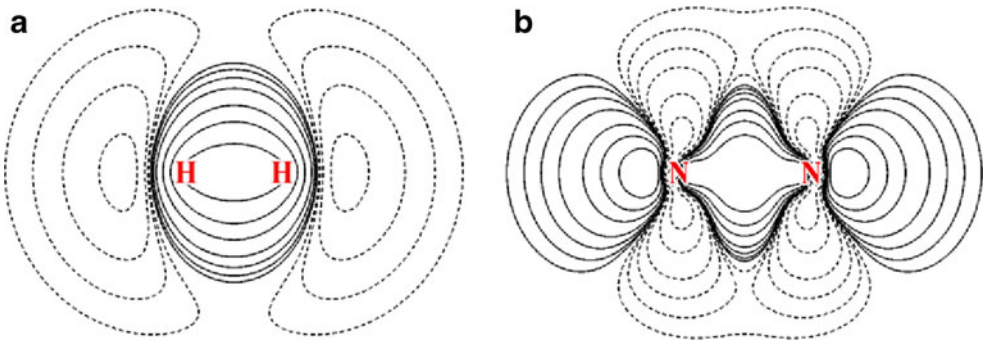

Fig. 4 Deformation map of electron density of **a** H_2 and **b** N_2. Solid and dashed lines correspond to the regions where electron density is increased and decreased in the formation process of the molecule, respectively

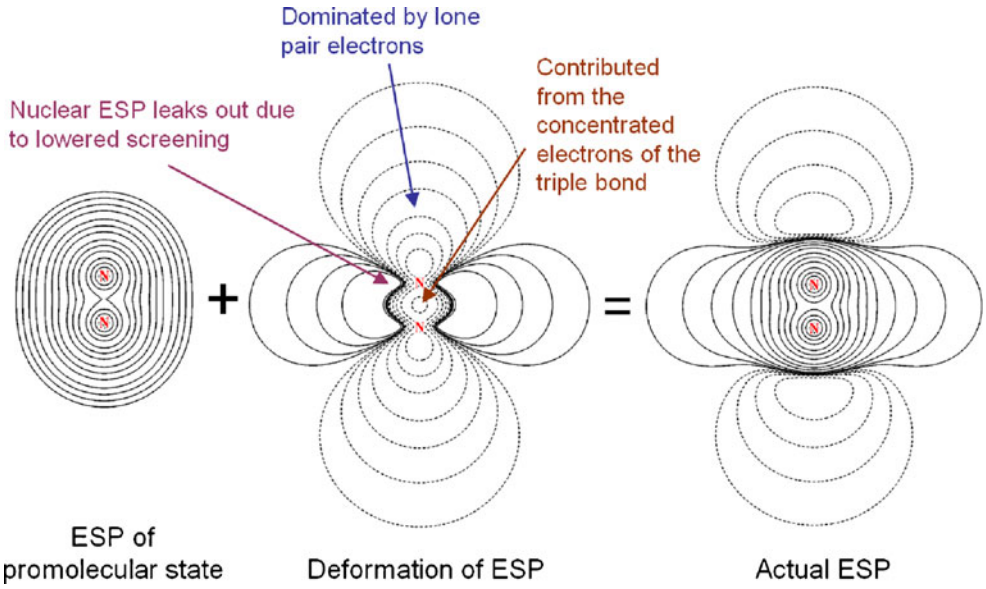

Fig. 5 Formation process of the actual ESP distribution of N_2. Solid and dashed lines correspond to positive and negative zones, respectively

electron density makes the positive ESP from nuclear charge leak out. This is the reason why N_2 has a torus-shaped positive ESP region encompassing its axis.

It is well know that molecules always tend to approach each other in a complementary manner of ESP to maximize electrostatic interaction energy. If we superpose the ESP contour map of the monomers according to monomer orientations in the dimers, then it is expected that the stability sequence of the dimer configurations could be well explained or predicted by simply visually examining the overlapping fashion and extent.

For Z configuration of $(N_2)_2$, it can be seen from Fig. 6 that there are two ESP complementary regions, where positive part of one N_2 and negative part of another N_2 overlap with each other significantly, suggesting that the electrostatic attraction between the two monomers is strong. This observation interprets why Z shape of $(N_2)_2$ is very stable. For T shape, there is only one ESP complementary zone between the two monomers, and the overlapping extent is smaller than that of Z, which results in a smaller inter-monomer interaction energy in comparison with that of Z. For X configuration, there simultaneously exists two small ESP complementary regions and a large ESP mutually exclusive region. In the latter, the ESPs of both monomers have the same sign and thus lead to electrostatic repulsion. Since the electrostatic attractive and repulsive effects cancelled each other to some degree, X shape is expected to have metastability. For both H and L configurations, the inter-monomer ESP overlapping is

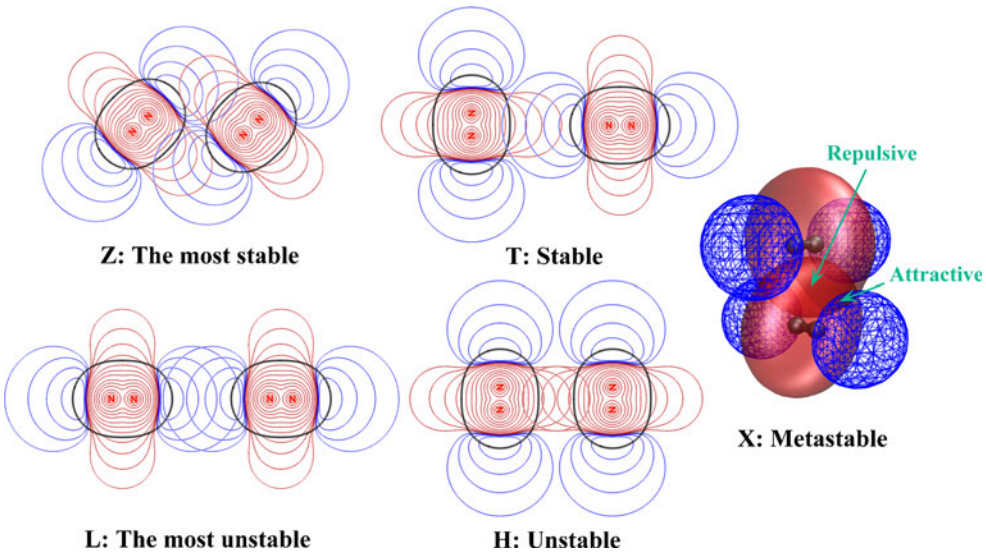

Fig. 6 Overlapping map of N_2 ESP. The marked configurational stabilities are measured relatively. For clarity, the graph of X configuration is shown in isosurface style, the isovalue is 0.003 a.u. for positive (red) and −0.0025 a.u. for negative (blue) parts

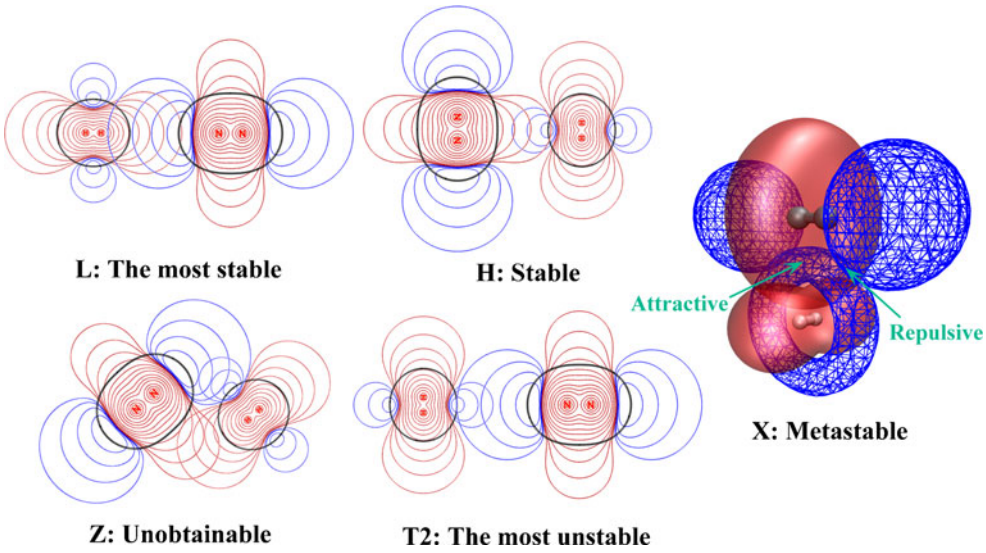

Fig. 7 Overlapping map of H_2 and N_2 ESP. The marked configurational stabilities are measured relatively. For clarity, the graph of X configuration is shown in isosurface style; the isovalue is 0.003 a.u. for positive (red) and −0.002 a.u. for negative (blue) parts

completely in mutually exclusive manner, and the overlapping extent is more prominent in L, therefore H should be relatively unstable and L should be the most unstable one. Our above ESP analyses reasonably and intuitively interpreted the stability sequence of $(N_2)_2$, namely T>Z>X>H>L. The case for $(H_2)_2$ is similar to $(N_2)_2$ and thus will not be discussed further here, one can find detail from Fig. S1.

Following the ESP analysis above, the configurational preference of $(H_2)(N_2)$ can also be successfully explained. As illustrated in Fig. 7, there is an ESP complementary region between H_2 and N_2 for both H and L configurations, hence H_2 and N_2 tend to arrange as H and L shapes as they approach each other. Since the overlapping region in L is evidently larger than that in H, L configuration is more stable than H configuration. In analogy with the case of $(N_2)_2$, X configuration of $(H_2)(N_2)$ is metastable due to the simultaneous presence of complementary (attractive) and mutually exclusive (repulsive) regions of ESP. T2 is expected to be the most unfavorable configuration since ESP of one monomer overlaps conspicuously with the ESP of another one with the same sign. As aforementioned, we were unable to obtain a Z configuration for $(H_2)(N_2)$ by the unconstrained optimization. The reason is that, as can be seen from Fig. 7, the mutual exclusion of monomer ESP for Z configuration is so severe that the electrostatic repulsion always drives the configuration to L shape.

It is interesting to note that the graphical analysis method we exemplified above is somewhat akin to the one involved in frontier molecular orbital (FMO) theory [37]. FMO theory states that the prerequisite for a favorable chemical reaction is that the HOMO and LUMO in the two molecules must be well matched with the same phase, while our graphical analysis showed that, in order to form a stable dimer, the ESP of the monomers should be substantially overlapped in different sign. We believe that this newly introduced ESP analysis method could also be used to explain or predict configurational stability of more complicated dimers or clusters. However, one should also be aware that the dispersion and polarization effects on configuration may be important for some other cases such as π-π stacking and strongly polar systems and hence should be taken into consideration carefully.

Conclusions

In conclusion, we studied inter-monomer interaction energies of $(H_2)_2$, $(N_2)_2$ and $(H_2)(N_2)$ at CCSD(T)/CBS level. DFT-SAPT energy decomposition analysis showed that the stability sequence of the dimer configurations is essentially controlled by the electrostatic interaction. This observation is somewhat contrary to the common belief in textbooks that these dimers are van der Waals complex, whose interaction is almost solely dominated by the dispersion effect. Moreover, via a graphical analysis method based on ESP, very vivid and definitive pictures were presented to answer the question on how the electrostatic interaction determines the configurational preference of the dimers. Quadrupole-quadrupole interaction model was assessed. Based on this approximate model the configurational preference of the dimers can also be partially explained, although it is not as intuitive as the graphical analysis presented above. In addition, by taking the CCSD(T)/CBS result as references, we benchmarked the performance of various theoretical methods. B3LYP-D3 is shown to be a cheap but relatively reliable method to evaluate the intermolecular interaction of $(H_2)_2$, $(N_2)_2$, and $(H_2)(N_2)$. Hence, this method is expected to be very useful in investigating large clusters or molecular crystals consisting of H_2 or N_2, which, on the other hand, may be difficult to be treated by expensive post-HF methods.

Acknowledgments The authors thank the National Natural Science Foundation of China (Project No. 21173020) for the financial support.

References

1. Burton PG, Senff UE (1982) J Chem Phys 76:6073–6087
2. Carmichael M, Chenoweth K, Dykstra CE (2004) J Phys Chem A 108:3143–3152
3. Diep P, Johnson JK (2000) J Chem Phys 112:4465–4473
4. Donchev AG, Galkin NG, Tarasov VI (2007) J Chem Phys 126: 174307–174310
5. Hobza P, Schneider B, Sauer J, Čársky P, Zahradník R (1987) Chem Phys Lett 134:418–422
6. Kochanski E (1973) J Chem Phys 58:5823–5831
7. Kochanski E, Roos B, Siegbahn P, Wood MH (1973) Theor Chem Accounts 32:151–159
8. Ree FH, Bender CF (1979) J Chem Phys 71:5362–5375
9. Senff UE, Burton PC (1989) Aust J Phys 42:47–58
10. Tapia O, Bessis G (1972) Theor Chem Accounts 25:130–137
11. Wind P, Røeggen I (1992) Chem Phys 167:263–275
12. Berns RM, van der Avoird A (1980) J Chem Phys 72:6107–6116
13. Böhm H-J, Ahlrichs R (1985) Mol Phys 55:1159–1169
14. van der Avoird A, Wormer PES, Jansen APJ (1986) J Chem Phys 84: 1629–1635
15. Uhlík F, Slanina Z, Hinchliffe A (1993) J Mol Struct (THEOCHEM) 282:271–275
16. Stallcop JR, Partridge H (1997) Chem Phys Lett 281:212–220
17. Wada A, Kanamori H, Iwata S (1998) J Chem Phys 109:9434–9438
18. Couronne O, Ellinger Y (1999) Chem Phys Lett 306:71–77
19. Jafari MHK, Maghari A, Shahbazian S (2005) Chem Phys 314:249–262
20. Gomez L, Bussery-Honvault B, Cauchy T, Bartolomei M, Cappelletti D, Pirani F (2007) Chem Phys Lett 445:99–107
21. Cappelletti D, Pirani F, Bussery-Honvault B, Gomez L, Bartolomei M (2008) Phys Chem Chem Phys 10:4281–4293
22. Salazar MC, Paz JL, Hernández AJ (1999) J Mol Struct (THEOCHEM) 464:183–189
23. Buryak I, Lokshtanov S, Vigasin A (2012) J Chem Phys 137: 114308–114308
24. Frisch MJ, Trucks GW, Schlegel HB, Scuseria GE, Robb MA, Cheeseman JR, Montgomery JA Jr, Vrevon T, Kudin KN, Burant JC, Millam JM, Iyengar SS, Tomasi J, Barone V, Menucci B, Cossi M, Scalmani G, Rega N, Petersson GA, Nakatsuji H, Hada M, Ehara M, Toyota K, Fukuda R, Hasegawa J, Ishida M, Nakajima T, Honda Y, Kitao O, Nakai H, Klene M, Li X, Knox JE, Hratchian HP, Cross JB, Adamo C, Jaramillo J, Gomparts R, Stratmann RE, Yazyev O, Austin AJ, Cammi R, Pomelli C, Ochterski JW, Ayala PY, Morokuma K, Voth GA, Salvador P, Dannenberg JJ, Zakrzewski VG, Dapprich S, Daniels AD, Strain MC, Farkas O, Malick DK, Rabuck AD, Raghavachari K, Foresman JB, Ortiz JV, Cui Q, Baboul AG, Clifford S, Cioslowski J, Stefanov BB, Liu G, Liashenko A, Piskorz P, Komaromi I, Martin RL, Fox DJ, Keith T, Al-Laham MA, Peng C-Y, Namayakkara A, Challacombe M, Gill PMW, Johnson B, Chen W, Wong M-W, Gonzalez C, Pople JA (2004) Gaussian 03, E.01st edn. Gaussian, Inc, Wallingford
25. Dunning JTH (1989) J Chem Phys 90:1007–1023
26. Kendall RA, Dunning TH, Harrison RJ (1992) J Chem Phys 96: 6796–6806
27. Papajak E, Truhlar DG (2010) J Chem Theory Comput 7:10–18
28. Halkier A, Helgaker T, Jørgensen P, Klopper W, Koch H, Olsen J, Wilson AK (1998) Chem Phys Lett 286:243–252
29. Boys SF, Bernardi F (1970) Mol Phys 19:553–566
30. Perdew JP, Burke K, Ernzerhof M (1996) Phys Rev Lett 77:3865–3868
31. Becke AD (1993) J Chem Phys 98:1372–1377
32. Zhao Y, Truhlar D (2008) Theor Chem Accounts 120:215–241
33. Peverati R, Truhlar DG (2011) J Phys Chem Lett 2:2810–2817
34. Grimme S, Antony J, Ehrlich S, Krieg H (2010) J Chem Phys 132: 154104–154119
35. Chai J-D, Head-Gordon M (2008) Phys Chem Chem Phys 10:6615–6620
36. Schmidt MW, Baldridge KK, Boatz JA, Elbert ST, Gordon MS, Jensen JH, Koseki S, Matsunaga N, Nguyen KA, Su S, Windus TL, Dupuis M, Montgomery JA (1993) J Comput Chem 14: 1347–1363
37. Jensen F (2007) Introduction to computational chemistry, 2nd edn. Wiley, Chichester
38. Stewart JP (2013) J Mol Model 19:1–32
39. MOPAC2012, James JP Stewart, Stewart Computational Chemistry, Version 13.159W web: HTTP://OpenMOPAC.net
40. MOLPRO, version 2008.1, a package of *ab initio* programs, Werner H-J, Knowles PJ, Lindh R, Manby FR, Schütz M and others, see http://www.molpro.net
41. Heßelmann A, Jansen G (2003) Chem Phys Lett 367:778–784
42. Heßelmann A, Jansen G (2003) Phys Chem Chem Phys 5:5010–5014
43. Adamo C, Barone V (1999) J Chem Phys 110:6158–6170
44. Multiwfn website: http://Multiwfn.codeplex.com. Accessed 10 Aug 2013
45. Lu T, Chen F (2012) J Comput Chem 33:580–592
46. Grimme S (2011) WIREs: Comput Mol Sci 1:211–228
47. Li Q, Yin P, Liu Y, Tang AC, Zhang H, Sun Y (2003) Chem Phys Lett 375:470–476
48. Kim C, Kim SJ, Lee Y, Kim Y (2000) Bull Korean Chem Soc 21: 510–514
49. Jaeger HM, Swenson DWH, Dykstra CE (2006) J Phys Chem A 110: 6399–6407
50. Buckingham AD (1959) Q Rev Chem Soc 13:183–214
51. Buckingham AD, Cordle JE (1974) Mol Phys 28:1037–1047
52. Birnbaum G, Cohen ER (1976) Mol Phys 32:161–167
53. Murray JS, Politzer P (2011) WIREs: Comput Mol Sci 1:153–163
54. Politzer P, Murray JS (1991) Molecular electrostatic potentials and chemical reactivity. In: Lipkowitz KB, Boyd DB (eds) Reviews in computational chemistry, vol 2. Wiley, New York, pp 273–312
55. Politzer P, Murray JS (2009) The electrostatic potential as a guide to molecular interactive behavior. In: Chattaraj PK (ed) Chemical reactivity theory: A density functional view. CRC, Boca Raton
56. Murray JS, Politzer P (1998) Electrostatic potentials: Chemical applications. Encyclopedia of computational chemistry, vol 2. Wiley, West Sussex
57. Lu T, Chen F (2012) J Mol Graph Model 38:314–323
58. Brinck T, Murray JS, Politzer P (1992) Mol Phys 76:609–617
59. Bader RFW, Carroll MT, Cheeseman JR, Chang C (1987) J Am Chem Soc 109:7968–7979